




Hydrostatic pressure-induced huge enhancement of critical current density and flux pinning in $\text{Fe}_{1-x}\text{Co}_x\text{Se}_{0.5}\text{Te}_{0.5}$ single crystals

Lina Sang^{1,2} , Babar Shabbir^{2,3}, Pankaj Maheshwari⁴, Wenbin Qiu², Zongqing Ma² , Shixue Dou², Chuanbing Cai¹, V P S Awana⁴  and Xiaolin Wang^{2,5}

¹ Shanghai Key Laboratory of High Temperature Superconductors, Physics Department, Shanghai University, Shanghai 200444, People's Republic of China

² Institute for Superconducting and Electronic Materials, Faculty of Engineering, Australian Institute for Innovative Materials, University of Wollongong, NSW 2500, Australia

³ College of Electronic Science and Technology, Shenzhen University, Shenzhen 518060, People's Republic of China

⁴ CSIR-National Physical Laboratory, Dr K S Krishnan Marg, New Delhi-110012, India

⁵ ARC Centre of Excellence in Future Low-Energy Electronics Technologies, University of Wollongong, Australia

E-mail: xiaolin@uow.edu.au

Received 11 July 2017, revised 24 November 2017

Accepted for publication 4 December 2017

Published 11 January 2018



Abstract

We performed a systematic study of the hydrostatic pressure (HP) effect on the superconducting transition temperature (T_c), critical current density (J_c), irreversibility field (H_{irr}), upper critical field (H_{c2}), and flux pinning mechanism in un-doped and 3 at.% Co-doped $\text{FeSe}_{0.5}\text{Te}_{0.5}$ crystals. We found that T_c is increased from 11.5 to 17 K as HP increases from 0 to 1.2 GPa. Remarkably, the J_c is significantly enhanced by a factor of 3 to 100 for low and high temperature and field, and the H_{irr} line is shifted to higher fields by HP up to 1.2 GPa. Based on the collective pinning model, the δl pinning associated with charge-carrier mean free path fluctuation is responsible for the pinning mechanism of $\text{Fe}_{1-x}\text{Co}_x\text{Se}_{0.5}\text{Te}_{0.5}$ samples with or without pressure. A comprehensive vortex phase diagram in the mixed state is constructed and analysed for the 3 at.% Co-doped sample.

Keywords: Fe-based superconductor, critical current density, flux pinning, upper critical field, irreversible field

(Some figures may appear in colour only in the online journal)

Introduction

Fe-based superconductors show great potential for carrying large currents and supporting high field magnet applications due to their high critical temperature, T_c , high upper critical field, H_{c2} , and irreversibility field, H_{irr} , and their low anisotropy [1–5]. Further enhancement of their critical current density, J_c , is still the main challenge from the

viewpoint of practical applications. So far, two main methods have been reported to enhance J_c by introducing point defects into Fe-based superconductors: chemical doping and high energy ion irradiation or implantation [6–10]. It is commonly observed that doping with various kinds of dopants can induce superconductivity and/or increase the flux pinning. However, high doping levels often degrade T_c and J_c . The density of point defects can be significantly

enriched by high energy ion treatment, which can lead to significant enhancement of J_c at high fields. The high energy dose, however, often causes T_c to decrease or disappear completely, which is also detrimental to J_c . Inspired by the study of pressure effects on T_c enhancement in Fe-based superconductors, we have recently proposed that hydrostatic pressure can also enhance both T_c and J_c for various Fe-superconducting systems. We have previously demonstrated that hydrostatic pressure (HP) can significantly increase the J_c in $\text{Sr}_4\text{V}_2\text{O}_6\text{Fe}_2\text{As}_2$ [11], $\text{NaFe}_{0.97}\text{Co}_{0.03}\text{As}$ [12], and $(\text{Ba}, \text{K})\text{Fe}_2\text{As}_2$ [13]. Obviously, HP has become the third effective approach to J_c and T_c enhancement for Fe-based superconductors, in addition to chemical doping and high energy radiation [14, 15]. Studies have shown that T_c increases from 38 to 50 K at 1.5 GPa for LaFeAsO_8 [16], from 15 to 22 K at 1.2 GPa for $\text{Sr}_4\text{V}_2\text{O}_6\text{Fe}_2\text{As}_2$ [11], from 11 to 21 K at 2.5 GPa for $\text{BaFe}_{1.92}\text{Co}_{0.08}\text{As}_2$ [17], from 20.4 to 31.0 K at 2.28 GPa for $\text{NaFe}_{0.972}\text{Co}_{0.028}\text{As}$ [18], from 8 to 37 K at 7 GPa for $\alpha\text{-FeSe}$ [19], and from 13.9 to 23.3 K at 3 GPa for $\text{Fe}_{1.03}\text{Se}_{0.57}\text{Te}_{0.43}$ [20]. Pressure has more advantages for the enhancement of J_c and flux pinning beyond the above-mentioned positive effect on T_c : (1) reducing the lattice parameters and shrinking the unit cells, leading to the reduction of anisotropy; (2) improving grain connectivity, overcoming the grain boundary weak-link problem; (3) introducing more pinning centers by increasing defects, causing a further increase in J_c , since the formation energy of point defects decreases with increasing pressure [21–23].

Previously, we have found that both self-field and high-field J_c increase greatly in $\text{NaFe}_{0.97}\text{Co}_{0.03}\text{As}$ single crystals and $\text{Sr}_4\text{V}_2\text{O}_6\text{Fe}_2\text{As}_2$ polycrystalline bulks as a result of HP, along with the T_c enhancement. It is worth pointing out that HP induces little change in T_c for $(\text{Ba}, \text{K})\text{Fe}_2\text{As}_2$, but it offers a significant enhancement in J_c , by at least 2 times for both low and high fields and temperatures. We have demonstrated that it is the point defects induced under high pressure that lead to significant improvement in J_c . In this work, we extend our study of the effects of hydrostatic pressure on superconductivity and J_c in $\text{FeSe}_{0.5}\text{Te}_{0.5}$ (11 phase) single crystals with or without doping. Due to their simple layered structure, isostructural FeSe and $\text{FeSe}_{0.5}\text{Te}_{0.5}$ are compounds that can provide clues to help us to understand the superconducting mechanism of the Fe-based superconductors. We demonstrate that HP has significant effects on T_c , J_c , H_{c2} , H_{irr} , and flux pinning in $\text{FeSe}_{0.5}\text{Te}_{0.5}$ (11-type) with/without cobalt doping. Remarkably, the enhancement in J_c is more than 250 times greater than without doping and pressure. We show that pressure introduces more pinning centers, reduces the anisotropy, and increases the superconducting volume and T_c . The flux pinning mechanism of samples is analyzed in terms of collective pinning theory, and it is found that the dominant pinning mechanism is δl pinning related to charge-carrier mean free path fluctuation.

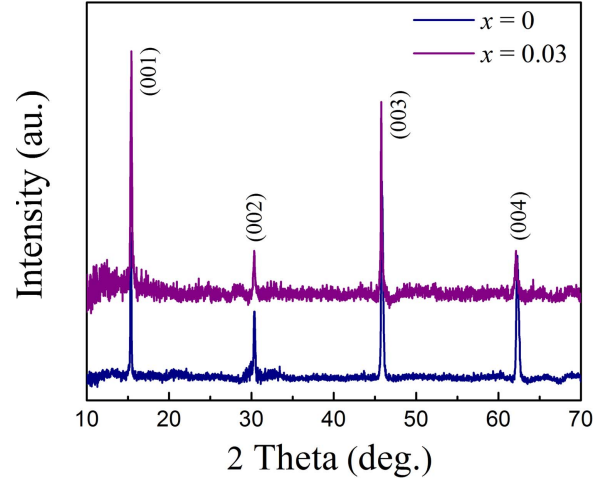


Figure 1. X-ray diffraction patterns of the un-doped and 3 at.% Co-doped samples.

Experimental details

Single crystals of $\text{Fe}_{1-x}\text{Co}_x\text{Se}_{0.5}\text{Te}_{0.5}$ were prepared by using the self-flux melt growth method. In our case, a stoichiometric mixture of Fe (Alfa Aesar, 99.99%), Se (Alfa Aesar, 99.99%), Te (Alfa Aesar, 99.99%), and Co (Alfa Aesar, 99.99%) powders were weighed, mixed, and ground thoroughly in an argon filled glove box. The powders were sealed in a quartz tube under argon and slowly heated to 450 °C, held for 4 h, and then the temperature was increased to 1000 °C at a rate of 2 °C min⁻¹, and then kept at that temperature for 24 h. Finally, the quartz ampule was cooled down to room temperature at a rate of 10 °C h⁻¹. We used an HMD high pressure cell and Daphne 7373 oil as the medium for applying hydrostatic pressure on our samples. Further details can be found in the pressure cell manual i.e. Quantum Design (QD) *High Pressure Cell User Manual* for use with the QD vibrating sample magnetometer (VSM). The magneto-transport was measured by the standard four-probe method with a physical properties measurement system (PPMS, Quantum Design) in the field range of 0–8 T, parallel to the *c*-axis. Magnetic measurements at different temperatures were performed on the Quantum Design PPMS by using the VSM. The J_c was calculated from the *M-H* data by the Bean model [24, 25], where $J_c = 20 \Delta M / Va(1 - a/3b)$, where *a* and *b* are the width and the length of the sample perpendicular to the applied field, respectively, *V* is the sample volume, and ΔM is the height difference in the *M-H* hysteresis loop. H_{irr} and H_{c2} were calculated from the 10% and 90% values of their corresponding resistivity transition from ρ_n (where ρ_n is the normal state resistivity just before the transition). H_{irr} is also obtained from the 10 A cm⁻² values the in J_c -*B* curves for various temperatures and pressures.

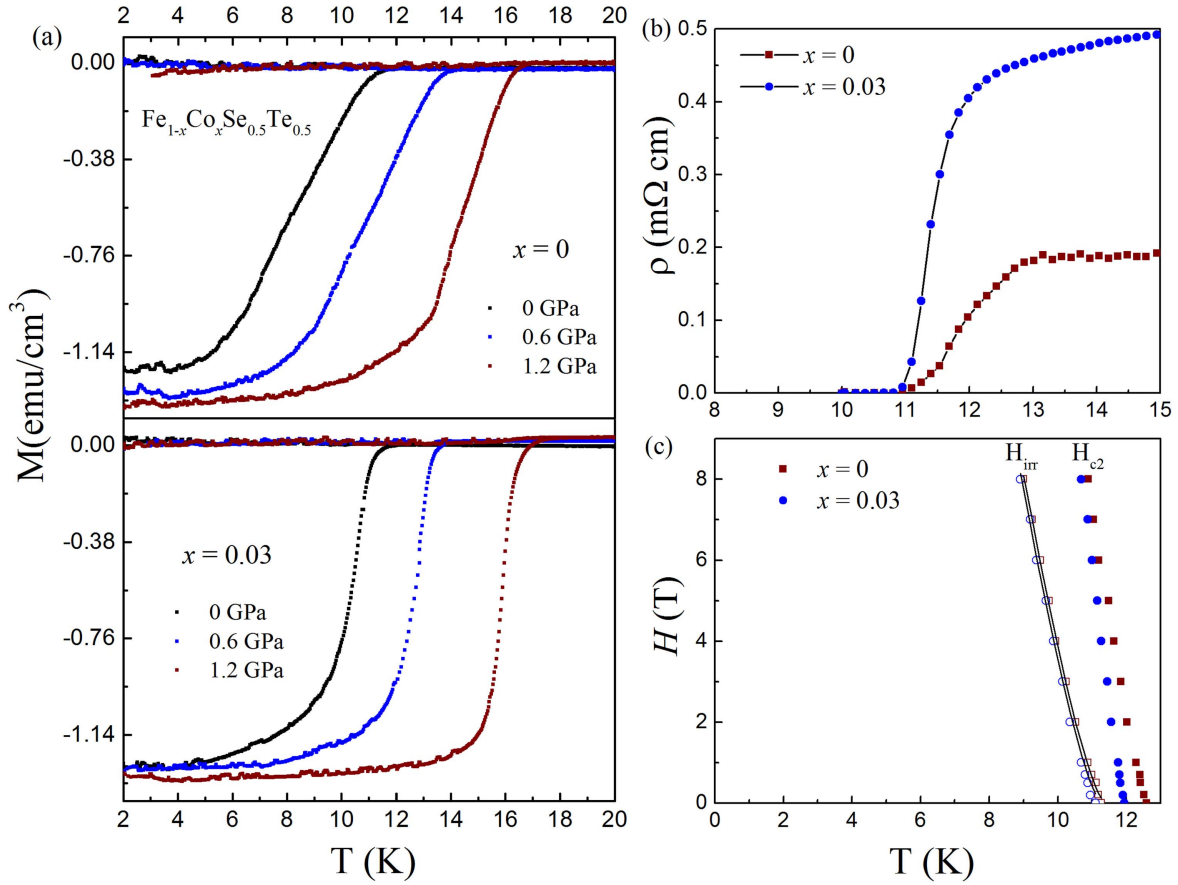


Figure 2. (a) Temperature dependence of zero-field-cooled and field-cooled (ZFC and FC) moments at different pressures for un-doped and 3 at.% Co-doped. (b) Resistivity versus temperature at zero field. (c) H_{c2} and H_{irr} versus temperature for the un-doped and 3 at.% Co-doped samples.

Results and discussions

Figure 1 shows the XRD pattern of $\text{Fe}_{1-x}\text{Co}_x\text{Se}_{0.5}\text{Te}_{0.5}$ ($x = 0.0$ and 0.03) single crystals. It is clearly seen that the crystal has (00 l) orientation and very narrow peak widths indicating high crystallinity of the studied crystals. Figure 2(a) shows the DC magnetization versus temperature (M - T) plot for un-doped and 3 at.% Co-doped samples measured at different pressures with 10 Oe parallel to the c -axis. Pressure enhanced the T_c from 11.5 to 17 K at 1.2 GPa for both samples. From the R - T curves, we found that T_c^{zero} of both samples are around 11 K (figure 2(b)) and obtained the H_{irr} lines (figure 2(c)). Figures 3(a)–(d) shows M - H loops measured at 0 and 1.2 GPa for both the un-doped and 3 at.% Co-doped samples. As can be seen, M - H loops are broadened greatly at both low and high fields compared to the loop without pressure, indicating that the broadening of the loops is caused by a big enhancement of the flux pinning due to the pressure.

J_c versus B curves for the un-doped and 3 at.% Co-doped samples at various temperatures for pressure $P = 0, 0.6$, and 1.2 GPa are shown in figures 4(a)–(d). At 2 K, the low-field J_c is strongly enhanced from 2×10^4 and 4.7×10^4 A cm $^{-2}$ at 0 GPa (black squares) to 1.15×10^5 and 1.53×10^5 A cm $^{-2}$ at

1.2 GPa (red triangles) for the un-doped and 3 at.% Co-doped samples, respectively. The J_c is significantly increased by over 100 times at high field and high temperature by pressure, which indicates that there is a great enhancement of the in-field performance. The critical current density as a function of magnetic field is measured at different temperatures. The straight lines are linear fitting of $J_c \sim B^{-n}$. H^* is determined by the crossing of the tangent to the inflection point and the low-field plateau, as shown in figure 4(c). Furthermore, the second magnetization peak, also called the fishtail effect [26–28], is present in the Co-doped samples and becomes very pronounced under pressure.

To quantify the J_c enhancement, the ratio of J_c ($x = 0.03$, 1.2 GPa)/ J_c ($x = 0$, 0 GPa) versus T at different fields is plotted as shown in figure 5(a). It can be seen that the ratio increases from 7.5 at 2 K to 51 at 10 K for zero field, from 17 at 2 K to 147 at 9 K for 1 T, from 19 at 2 K up to 231 at 8 K for 3 T, and from 21 at 2 K to 440 at 7 K for 7 T, respectively. The values of $J_c^{1.2\text{GPa}}/J_c^{0\text{GPa}}$ versus temperature at 0 T and 7 T for un-doped and 3 at.% Co-doped samples are plotted in figure 5(b), where the ratio increases from 3 to 300 for the 3 at.% Co-doped sample. These data show that the pressure-induced enhancement in J_c is remarkable in the 3 at.% Co-doped sample at both high field and high temperature, and the higher the field is, the larger the J_c enhancement will be.

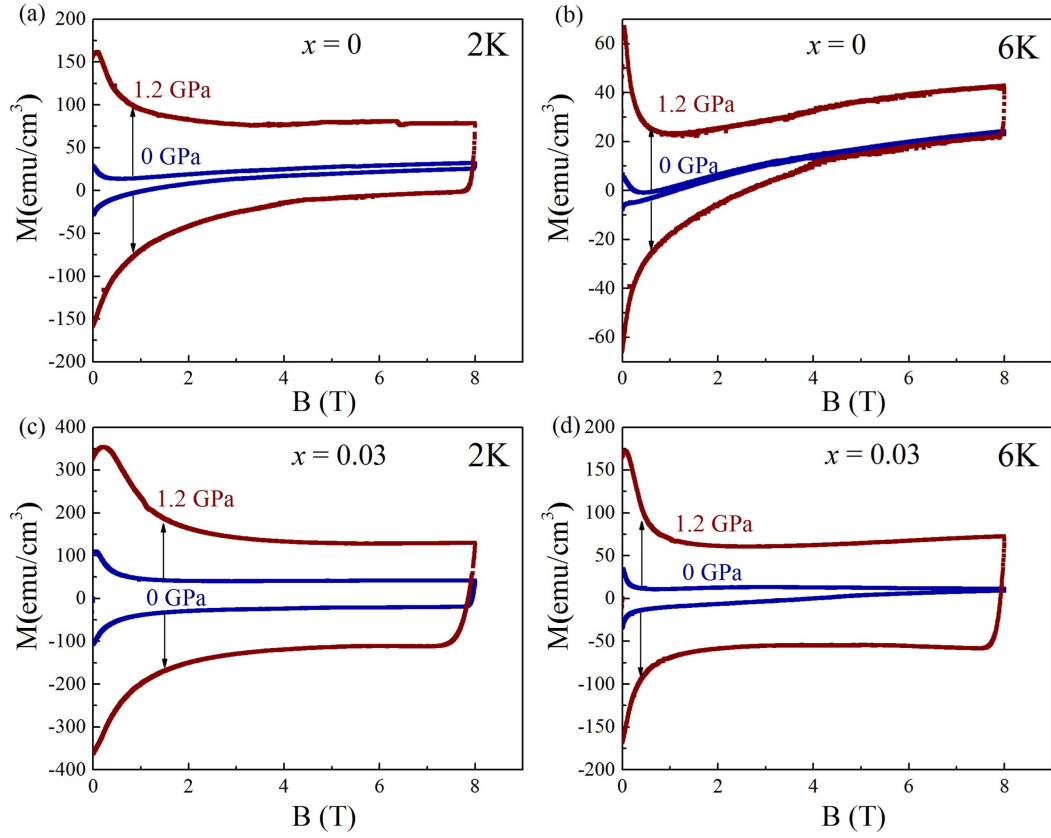


Figure 3. M - H measurements of un-doped and 3 at.% Co-doped samples at 2 and 6 K.

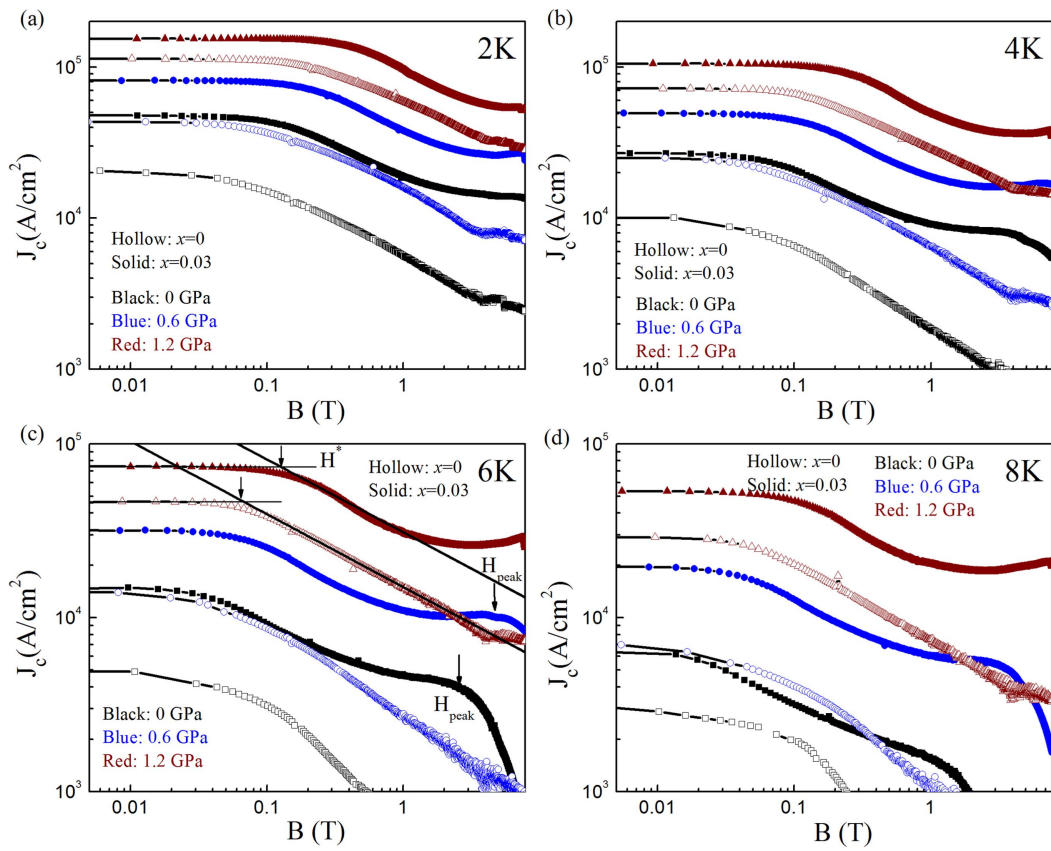


Figure 4. J_c versus field under different pressures at 2, 4, 6, and 8 K for the un-doped and 3 at.% Co-doped.

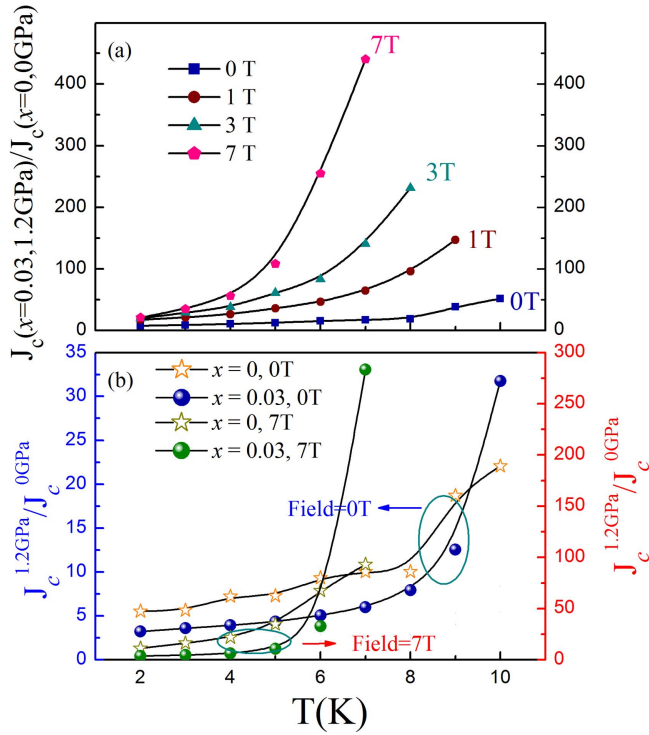


Figure 5. (a) The ratio of $J_c(x = 0.03, 1.2 \text{ GPa})/J_c(x = 0, 0 \text{ GPa})$ versus temperature at different fields. (b) The ratio of $J_c(1.2 \text{ GPa})/J_c(0 \text{ GPa})$ versus temperature at 0 T and 7 T for the un-doped and 3 at.% Co-doped samples.

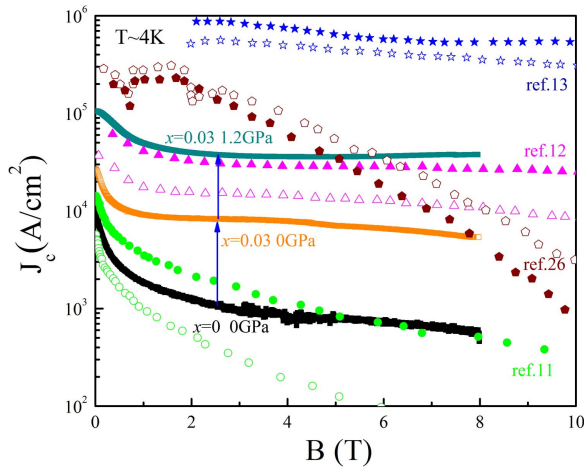


Figure 6. J_c versus B for un-doped sample at 0 GPa and 3 at.% Co-doped sample at 0 and 1.2 GPa, compared with (Ba, K)Fe₂As₂ [13], NaFe_{0.97}Co_{0.03}As [12], Sr₄V₂O₆Fe₂As₂ [11], and MgB₂ [29]. Hollow symbols represent results under atmospheric pressure, solid symbols represent results under pressure.

As a comparison, the J_c for NaFe_{0.97}Co_{0.03}As, Sr₄V₂O₆Fe₂As₂, and (Ba, K)Fe₂As₂ with and without pressure are given in figure 6 [11–13]. J_c is also enhanced for the Ba_{0.6}K_{0.4}Fe₂As₂ crystal, but the T_c of 37.9 K does not change under pressure. Additionally, the T_c and J_c are slightly reduced at low field, and they drop very quickly at high field

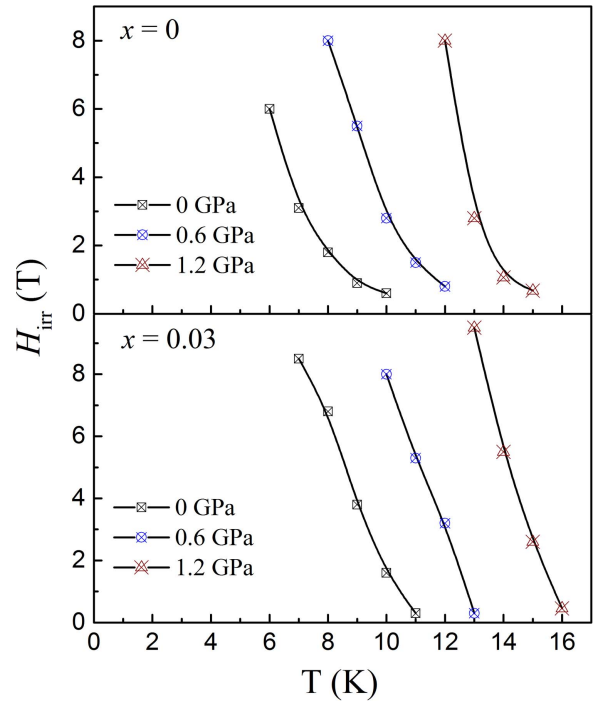


Figure 7. Plot of H_{irr} versus temperature at different pressures for un-doped and 3 at.% Co-doped samples.

under pressure for MgB₂ [29]. We found that the J_c of 3 at.% Co-doped sample shows the greatest increase at the same pressure and reaches higher values at both low and high field. The highest J_c at 1.2 GPa and 4 K is higher than for NaFe_{0.97}Co_{0.03}As at both low and high fields, and much higher than that of MgB₂ for $B > 6 \text{ T}$. H_{irr} was determined by a linear extrapolation down to 10 A cm^{-2} of the $J_c \sim B$ curves. Beside the great enhancement of J_c , we found that the H_{irr} of the un-doped and 3 at.% Co-doped samples are significantly improved by pressure, as shown in figure 7.

Now, let us discuss the possible flux pinning mechanisms for the pressure-induced significant enhancement of J_c in the un-doped and 3 at.% Co-doped samples. According to the Ginzburg–Landau theory, J_c obeys the power law $J_c \propto (1 - T/T_c)^\beta$ [30, 31], so we can distinguish different vortex pinning mechanisms depending on the different exponents β . It has been verified that $\beta = 1$ corresponds to individual, non-interacting vortices and $\beta > 1.5$ matches effective and strong vortex core pinning [12, 32]. Figures 8(a), (b) show J_c versus $(1 - T/T_c)$ at different pressures and fields using double logarithmic scaling. We find that the exponent β ranges from 1.88 and 1.9 at $P = 0 \text{ GPa}$, to 2 and 1.66 at $P = 1.2 \text{ GPa}$ for the un-doped and 3 at.% Co-doped samples at 0 T, as shown in figure 8(a). Figure 8(b) shows that β drops from 5.6 and 5 at $P = 0 \text{ GPa}$ down to 4.1 and 2 at $P = 1.2 \text{ GPa}$ for the un-doped and 3 at.% Co-doped samples at 7 T. This indicates that the exponent $\beta > 1.5$ shows strong and effective vortex core pinning for both samples. In addition, the relatively low values of β at

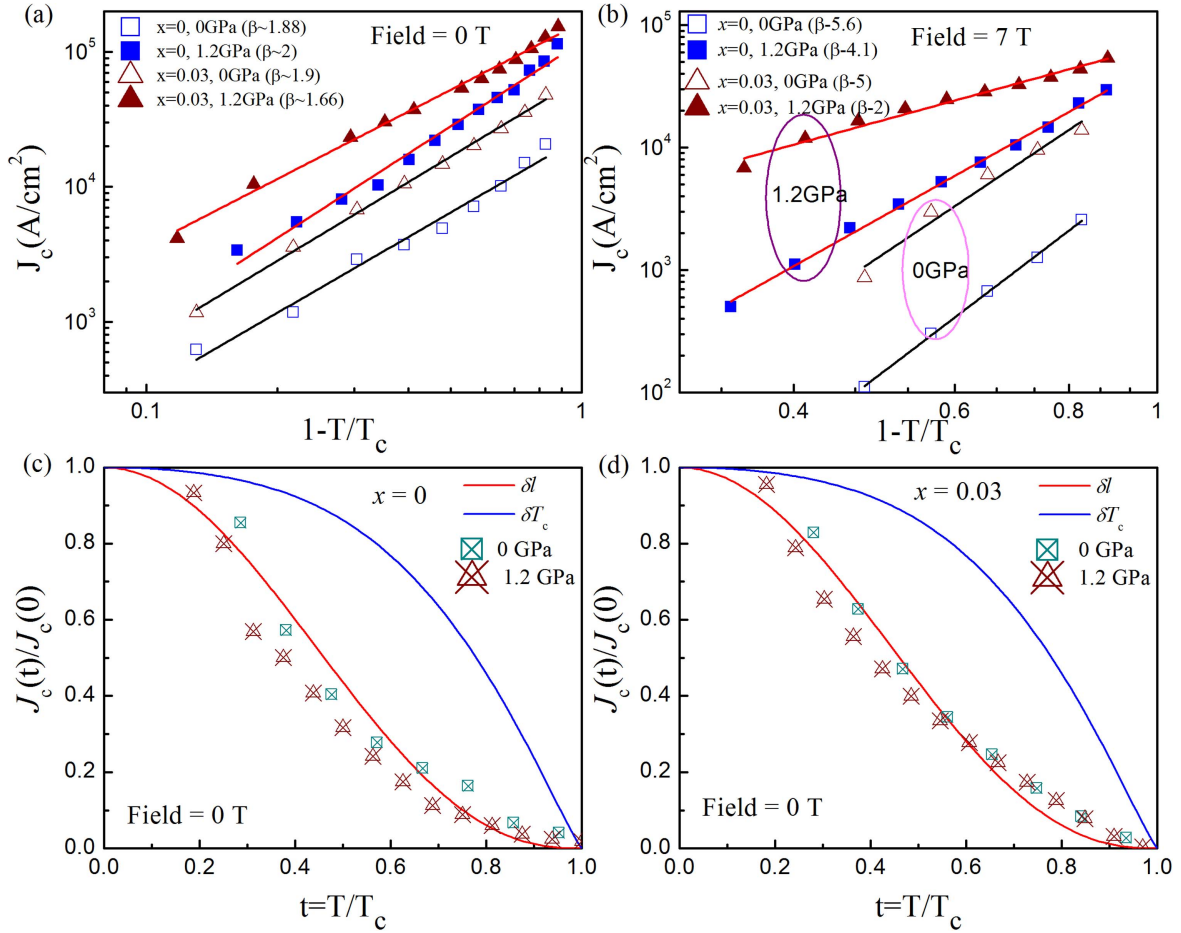


Figure 8. Logarithmic plot of J_c versus $(1 - T/T_c)$ at (a) 0 T and (b) 7 T under different pressures for the un-doped and 3 at.% Co-doped samples. Normalized measured J_c versus $t = T/T_c$ under different pressures for the (c) un-doped and (d) 3 at.% Co-doped samples, in good agreement with δl pinning.

$P = 1.2$ GPa show that the J_c drops relatively slowly, in contrast to its values at atmospheric pressure.

We further analysed our data using collective pinning theory. It is generally known that there are two main core pinning mechanisms, relating to variations in the critical temperature (δT_c) and the mean free path (δl), which display a different behavior of J_c versus temperature in the single vortex pinning regime. They obey the following equations (1) and (2):

$$\delta T_c \text{ pinning: } J_c(t)/J_c(0) = (1 - t^2)^{7/6}(1 + t^2)^{-6/5} \quad (1)$$

$$\delta l \text{ pinning: } J_c(t)/J_c(0) = (1 - t^2)^{5/2}(1 + t^2)^{-1/2} \quad (2)$$

where $t = T/T_c$ [33, 34].

The $J_c(t)$ values have been obtained from the J_c - B curves, and the calculated values of $J_c(t)/J_c(0)$ in the cases of δT_c pinning and δl pinning are displayed by the solid curves. In figures 8(c) and (d), the behavior of $J_c(t)/J_c(0)$ versus $t = T/T_c$ is well described by the δl pinning mechanism for both the un-doped and the 3 at.% Co-doped samples at 0 and 1.2 GPa, suggesting that there is single vortex pinning due to spatial variations in the charge-carrier mean free path l [26, 35].

The pinning force ($F_p = J_c \times B$) versus field curves for the un-doped and 3 at.% Co-doped samples at 2, 4, and 7 K are plotted in figure 9. It can be clearly observed that the F_p value for the 3 at.% Co-doped sample is enhanced significantly compared with the un-doped sample. This indicates that the doping increases the number of point pinning centers, leading to an enhanced total pinning force (figure 9(b)). Pressure can further increase the amount of pinning centers and the pinning force strength, giving rise to significant J_c enhancement, as shown in figures 9(c), (d). At high field and pressure, the F_p value for the 3 at.% Co-doped sample is more than 20 times greater than that of the un-doped sample at 0 GPa at 2 K.

According to the Dew-Hughes model, $F_p \propto h^m(1 - h)^n$, where $h = H/H_{irr}$, different m and n fitting parameters define the specific pinning mechanism. In this classical model, the exponents $m = 1$ and $n = 2$ represent point pinning, while $m = 1/2$ and $n = 2$ represent surface pinning, as was predicted by Kramer. In figure 10(a), we found that the experimental data fit nicely into the point pinning mechanism at 8 K for $P = 0$ GPa. The best fit of the curves is obtained with an $f(h)$ dependence given by $h^{1.5}(1 - h)^3$ for $P = 1.2$ GPa, as

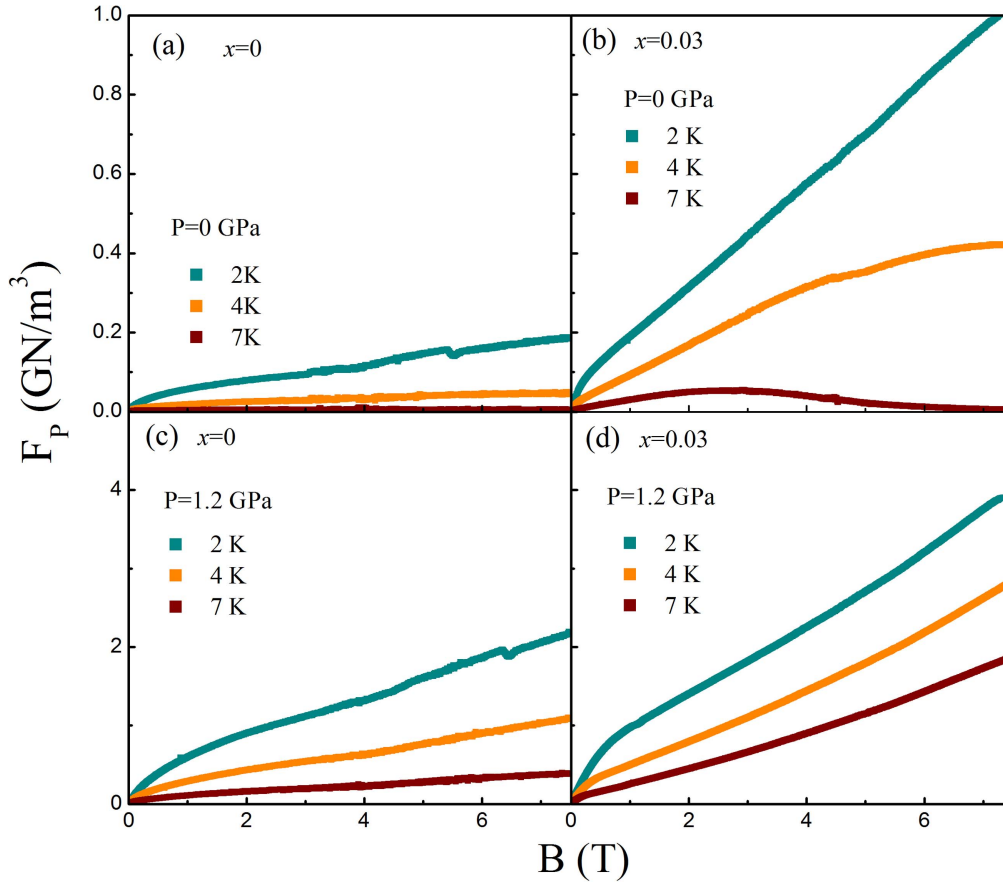


Figure 9. Field dependence of F_p (a), (b) at $P = 0$ GPa and (c), (d) at $P = 1.2$ GPa for the un-doped and 3 at.% Co-doped samples.

shown in figure 10(b). The obtained $m = 1.5$ and $n = 3$ are similar to the reported values of $m = 1.35$ and $n = 3.06$ in $\text{Fe}_{1.04}\text{Te}_{0.6}\text{Se}_{0.4}$ [36]. In the Dew-Hughes model, it should be noted that $h_{\text{max}} (=m/(m+n)) = 0.2$ corresponds to surface pinning for normal center of core interaction, while $h_{\text{max}} = 0.33$ corresponds to point core pinning [37, 38]. In the case of this sample under pressure, h_{max} is 0.34 and it corresponds to small size normal point pinning.

To figure out whether or not pressure can induce extra point defects, let us discuss peak effect in the sample with or without pressure. The peak or ‘fishtail’ effect is caused by the matching of the spacing between defects with the vortex lattice spacing for a certain magnetic field (matching field). If no extra pinning centers are induced by pressure, the matching field should remain the same. If the pinning energy for each pinning center is increased, we should expect that the peak height (J_c at the matching field) should increase. However, this is not the case in our results. We can see from figure 4(c) that the matching field gradually shifts to high field with pressure. Obviously, extra pinning centers should be induced under pressure. We have calculated the intervortex distance d for the cases with or without pressure. The intervortex distance is known to be dependent on the applied magnetic field: $d \approx (\Phi_0/B)^{0.5}$, where d is the intervortex distance and Φ_0 is the quantum of magnetic flux (2.068×10^{-15} Wb). We found that d decreases from 30 nm ($P = 0$ GPa)

to 15 nm ($P = 1.2$ GPa) indicating that high pressure can indeed increase point defect density greatly.

We plot the vortex phase diagrams for the 3 at.% Co-doped sample at $P = 0$ and 1.2 GPa, as shown in figure 11. The crossover field H^* and H_{peak} were obtained via the plots of J_c versus B (see figure 4(c)), where H^* is determined by the crossing of the tangent $J_c \sim B^{-n}$ to the inflection point and the low-field plateau. H_{irr} was also calculated from the $J_c = 10 \text{ A cm}^{-2}$ values in the J_c - B plots. H_{c2} values were obtained from the 90% values of their appropriate resistivity transitions. From the diagram, we can see that the vortex creep suddenly becomes faster and enters the plastic creep regime [26, 33, 39–43]. According to the collective pinning theory, the magnetic field dependence of J_c obeys different laws. When the applied field is below H^* , the J_c is field independent, with a single vortex-pinning mechanism dominating the vortex lattice. While J_c decreases quickly above H^* , it follows a power law, consistent with the small-bundle-pinning regime [33, 42, 44]. Hence, the diagram can be clearly divided into five regions according to the strength of the applied field. (I) Single vortex pinning, which is defined below H^* . (II) Small bundle pinning, which governs the region between H^* and H_{peak} . (III) Plastic creep, which holds between H_{peak} and H_{irr} . (IV) Vortex liquid, which is the dominant regime from H_{irr} to H_{c2} . (V) Normal state, which is above H_{c2} . It is important to note that the lines of H^* , H_{irr} , and

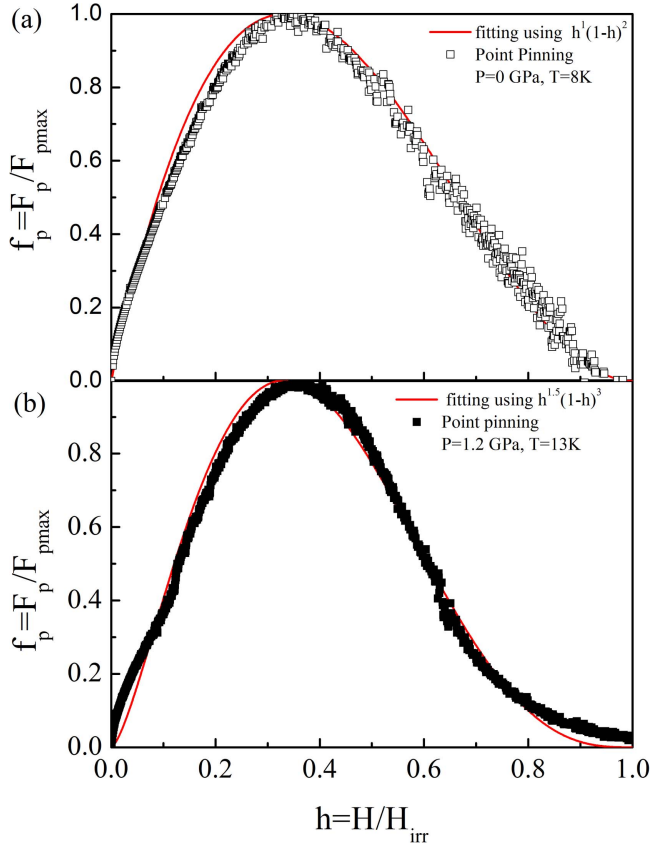


Figure 10. Plots of f_p versus H/H_{irr} at $P = 0$ GPa and $P = 1.2$ GPa for the 3 at.% Co-doped sample, in good agreement with point pinning.

H_{peak} are significantly increased by pressure, as shown in figure 11(b). The enhancement of H^* by pressure indicates that the maximum J_c survives to higher fields. The enhancement of H_{irr} shows the great improvement in in-field J_c performance.

Conclusion

We have systematically investigated the effects of HP on T_c , J_c , H_{irr} and H_{c2} , and flux pinning in $Fe_{1-x}Co_xSe_{0.5}Te_{0.5}$ single crystals. We found that HP can induce huge enhancement of the critical current density and flux pinning. The T_c increases from 11.5 at 0 GPa to 17 K at 1.2 GPa for the un-doped and 3 at.% Co-doped samples. The J_c is improved by at least five times at low field and more than a hundredfold for high field. Our results indicate that more point pinning centres are induced with pressure. The dominant pinning mechanism is δI pinning.

Acknowledgments

X L W acknowledges support from the Australian Research Council (ARC) through an ARC Discovery Project (DP130102956) and an ARC Professorial Future Fellowship project (FT130100778). This work was also supported in part

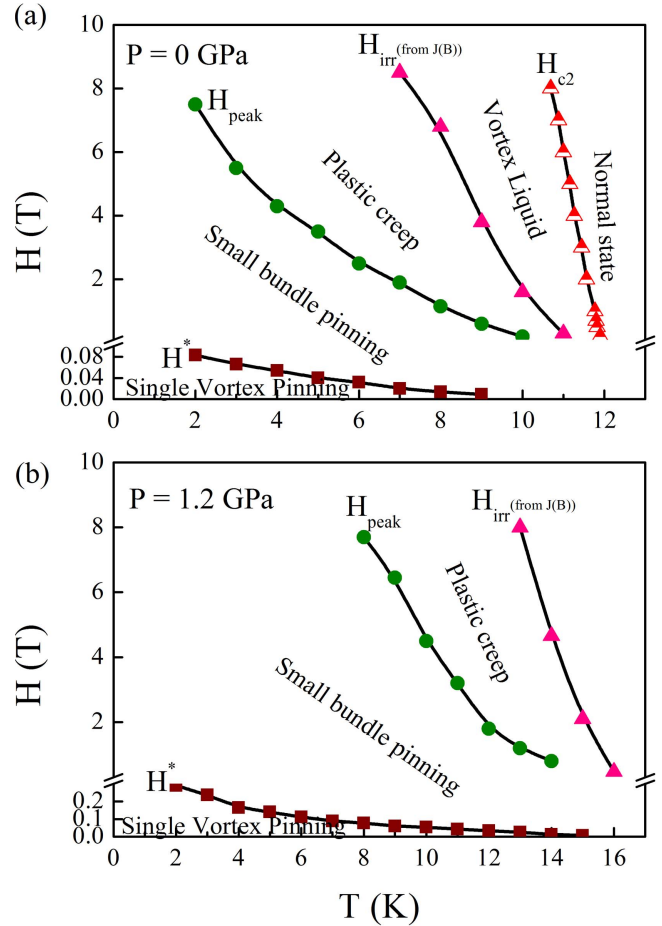


Figure 11. Vortex phase diagram for 3 at.% Co-doped sample at $P = 0$ GPa and $P = 1.2$ GPa. H^* , H_{peak} , and H_{irr} were obtained from the experimental $J_c(B)$ curves (see figure 4).

by the Science and Technology Commission of Shanghai Municipality (16521108400, 16DZ0504300 and 14521102800), the National Natural Science Foundation of China (51572165, and 11174193 and 51202141), and the National Key R&D Program (2016YFF0101701). L N S is grateful to the China Scholarship Council (CSC) for providing her PhD scholarship. Dr T. Silver's critical reading of this paper is greatly appreciated.




Author contributions

X L W conceived the research and designed the experiments. L N S performed all the measurements. L N S, X L W, B S, C B C, S X D, W B Q and Z Q M, analysed the data. P K M and V P S A prepared the samples. L N S and X L W wrote the paper.

Additional information

Competing interests: The authors declare that they have no competing interests.

ORCID iDs

Lina Sang  <https://orcid.org/0000-0002-6663-1265>
 Zongqing Ma  <https://orcid.org/0000-0002-3370-9441>
 V P S Awana  <https://orcid.org/0000-0002-4908-8600>

References

- [1] Kamihara Y, Watanabe T, Hirano M and Hosono H 2008 *J. Am. Chem. Soc.* **130** 3296
- [2] Wang X-L, Ghorbani S R, Lee S-I K, Dou S X, Lin C T, Johansen T H, Müller K-H, Cheng Z X, Peleckis G and Shabazi M 2010 *Phys. Rev. B* **82** 024525
- [3] Wang X, Ghorbani S R, Peleckis G and Dou S 2009 *Adv. Mater.* **21** 236
- [4] Moll P J W, Puzniak R, Balakirev F, Rogacki K, Karpinski J, Zhigadlo N D and Batlogg B 2010 *Nat. Mater.* **9** 628
- [5] Ni N, Bud'ko S L, Kreyssig A, Nandi S, Rustan G E, Goldman A I, Gupta S, Corbett J D, Kracher A and Canfield P C 2008 *Phys. Rev. B* **78** 014507
- [6] Prozorov R, Kończykowski M, Tanatar M A, Thaler A, Bud'ko S L, Canfield P C, Mishra V and Hirschfeld P J 2014 *Phys. Rev. X* **4** 041032
- [7] Sun Y, Park A, Pyon S, Tamegai T, Kambara T and Ichinose A 2017 *Phys. Rev. B* **95** 104514
- [8] Nakajima Y, Tsuchiya Y, Taen T, Tamegai T, Okayasu S and Sasase M 2009 *Phys. Rev. B* **80** 012510
- [9] Kim H, Gordon R T, Tanatar M A, Hua J, Welp U, Kwok W K, Ni N, Bud'ko S L, Canfield P C and Vorontsov A B 2010 *Phys. Rev. B* **82** 060518
- [10] Tanatar M A, Reid J-P H, Shakeripour H, Luo X G, Doiron-Leyraud N, Ni N, Bud'ko S L, Canfield P C, Prozorov R and Taillefer L 2010 *Phys. Rev. Lett.* **104** 067002
- [11] Shabbir B, Wang X, Ghorbani S R, Shekhar C, Dou S and Srivastava O N 2015 *Sci. Rep.* **5** 8213
- [12] Shabbir B, Wang X, Ghorbani S R, Wang A F, Dou S and Chen X H 2015 *Sci. Rep.* **5** 10606
- [13] Shabbir B, Wang X, Ma Y, Dou S X, Yan S-S and Mei L-M 2016 *Sci. Rep.* **6** 23044
- [14] Jung S-G, Kang J-H, Park E, Lee S, Lin J-Y, Chareev D A, Vasiliev A N and Park T 2015 *Sci. Rep.* **5** 16385
- [15] Takahashi H, Igawa K, Arii K, Kamihara Y, Hirano M and Hosono H 2008 *Nature* **453** 376
- [16] Yi W, Zhang C, Sun L, Ren Z-A, Lu W, Dong X, Li Z, Che G, Yang J and Shen X 2009 *Europhys. Lett.* **84** 67009
- [17] Ahilan K, Balasubramaniam J, Ning F L, Imai T, Sefat A S, Jin R, McGuire M A, Sales B C and Mandrus D 2008 *J. Phys. Condens. Matter* **20** 472201
- [18] Wang A F, Xiang Z J, Ying J J, Yan Y J, Cheng P, Ye G J, Luo X G and Chen X H 2012 *New J. Phys.* **14** 113043
- [19] Margadonna S, Takabayashi Y, Ohishi Y, Mizuguchi Y, Takano Y, Kagayama T, Nakagawa T, Takata M and Prassides K 2009 *Phys. Rev. B* **80** 064506
- [20] Gresty N C, Takabayashi Y, Ganin A Y, McDonald M T, Claridge J B, Giap D, Mizuguchi Y, Takano Y, Kagayama T and Ohishi Y 2009 *J. Am. Chem. Soc.* **131** 16944
- [21] Kuklja M M and Kunz A B 1999 *J. Appl. Phys.* **86** 4428
- [22] Lontos C A, Potsidi M S, Bak-Misiuk J, Misiuk A and Emtsev V V 2003 *Cryst. Res. Technol.* **38** 1058
- [23] Misiuk A 2000 *Mater. Phys. Mech.* **1** 119
- [24] Chen D-X, Sanchez A, Nogues J and Muoz J S 1990 *Phys. Rev. B* **41** 9510
- [25] Ravi Kumar G and Chaddah P 1989 *Phys. Rev. B* **39** 4704
- [26] Das P, Thakur A D, Yadav A K, Tomy C V, Lees M R, Balakrishnan G, Ramakrishnan S and Grover A K 2011 *Phys. Rev. B* **84** 214526
- [27] Pramanik A K, Harnagea L, Nacke C, Wolter A U B, Wurmehl S, Kataev V and Büchner B 2011 *Phys. Rev. B* **83** 094502
- [28] Werner M, Sauerzopf F M, Weber H W and Wisniewski A 2000 *Phys. Rev. B* **61** 14795
- [29] Shabbir B, Wang X L, Ghorbani S R, Dou S X and Xiang F 2015 *Supercond. Sci. Technol.* **28** 055001
- [30] Brück S and Albrecht J 2005 *Phys. Rev. B* **71** 174508
- [31] Djupmyr M, Cristiani G, Habermeyer H-U and Albrecht J 2005 *Phys. Rev. B* **72** 220507
- [32] Djupmyr M, Soltan S, Habermeyer H-U and Albrecht J 2009 *Phys. Rev. B* **80** 184507
- [33] Blatter G, Feigel'man M V, Geshkenbein V B, Larkin A I and Vinokur V M 1994 *Rev. Mod. Phys.* **66** 1125
- [34] Griessen R, Hai-Hu W, Van Dalen A J J, Dam B, Rector J, Schnack H G, Libbrecht S, Osquiguil E and Bruynseraede Y 1994 *Phys. Rev. Lett.* **72** 1910
- [35] Cai C, Holzapfel B, Hänisch J, Fernandez L and Schultz L 2004 *Phys. Rev. B* **69** 104531
- [36] Shabazi M, Wang X L, Dou S X, Fang H and Lin C T 2013 *J. Appl. Phys.* **113** 17E115
- [37] Wu Z F, Wang Z H, Tao J, Qiu L, Yang S G and Wen H H 2016 *Supercond. Sci. Technol.* **29** 035006
- [38] Yadav C S and Paulose P L 2011 *Solid State Commun.* **151** 216
- [39] Prozorov R, Ni N, Tanatar M A, Kogan V G, Gordon R T, Martin C, Blomberg E C, Pommpan P, Yan J Q and Bud'ko S L 2008 *Phys. Rev. B* **78** 224506
- [40] Sun Y, Pyon S, Tamegai T, Kobayashi R, Watashige T, Kasahara S, Matsuda Y and Shibauchi T 2015 *Phys. Rev. B* **92** 144509
- [41] Abulafia Y, Shaulov A, Wolfus Y, Prozorov R, Burlachkov L, Yeshurun Y, Majer D, Zeldov E, Wühl H and Geshkenbein V B 1996 *Phys. Rev. Lett.* **77** 1596
- [42] Ghorbani S R, Wang X L, Dou S X, Lee S-I and Hossain M S A 2008 *Phys. Rev. B* **78** 184502
- [43] Xiang F X, Wang X L, Xun X, De Silva K S B, Wang Y X and Dou S X 2013 *Appl. Phys. Lett.* **102** 152601
- [44] Ghorbani S R, Wang X-L, Hossain M S A, Yao Q W, Dou S X, Lee S-I K, Chung K C and Kim Y K 2010 *J. Appl. Phys.* **107** 113921